Article

Neural differentiation dynamics controlled by multiple feedback loop motifs in a comprehensive molecular interaction network

Tsuyoshi Iwasaki[1,2], Ryo Takiguchi[2], Takumi Hiraiwa[2], Takahiro G. Yamada[2], Kazuto Yamazaki[1], Noriko Hiroi[2,3,*], Akira Funahashi[2]

[1] Research Division, Sumitomo Dainippon Pharma. Co. Ltd, Osaka, Osaka, Japan
[2] Department of Biosciences and Informatics, Keio University, Yokohama, Kanagawa, Japan
[3] Faculty of Pharmaceutical Sciences, Sanyo-Onoda City University, Yamaguchi, Japan
[*] Correspondence: hiroi@rs.socu.ac.jp

Abstract: Computational simulation using mathematical models is a useful method for understanding the complex behavior of a living system. The majority of studies using mathematical models to reveal biological mechanisms uses one of the two main approaches: the bottom-up or the top-down approach. When we aim to analyze a large-scale network, such as a comprehensive knowledge-integrated model of a target phenomenon, for example a whole-cell model, the variation of analyses is limited to particular kind of analysis because of the size and complexity of the model. To analyze a large-scale regulatory network of neural differentiation, we developed a hybrid method that combines both approaches. To construct a mathematical model, we extracted network motifs, subgraph structures that recur more often in a metabolic network or gene regulatory network than in a random network, from a large-scale regulatory network, detected regulatory motifs among them, and combined these motifs. We confirmed that the model reproduced the known dynamics of HES1 and ASCL1 before and after differentiation, including oscillation and equilibrium of their concentrations. The model also reproduced the effects of overexpression and knockdown of the Id2 gene. Our model suggests that the characteristic change in HES1 and ASCL1 expression in the large-scale regulatory network is controlled by a combination of four feedback loops, including a large loop which has not been focused on. The model extracted by our hybrid method has the potential to reveal the critical mechanisms of neural differentiation. The hybrid method is applicable to other biological events.

Keywords: neural differentiation; regulatory motif; feedback regulation; signaling pathway; mathematical models

1. Introduction

Computational simulation using mathematical models is useful for understanding complex systems. Mathematical models of biological mechanisms use either the bottom-up or top-down approach [1]. Both approaches have their own challenges. The bottom-up approach has problems in acquiring regulatory relationships, whereas the top-down approach has problems in parameter determination. In the bottom-up approach, a few molecules of interest may be the pivot of an extended molecular network underlying the target biological event. For example, a mathematical model of the budding yeast cell cycle has been constructed using the bottom-up approach by combining known biochemical reactions [2]. This approach could yield a widely applicable model to simulate each specific analysis subject, but it is difficult to apply to the analysis of comprehensive biochemical networks because of limited information on the regulatory interactions of molecules and the parameters of mathematical models. The top-down approach is used to determine the intrinsic control mechanisms of target biological events. A simple model that simulates characteristic local dynamics is constructed using pathway databases or in a data-driven manner based on omics data by excluding non-essential factors from a comprehensive network. In the absence of a comprehensive

pathway map, a statistical model is one of the first choices to construct a comprehensive network [3–5]. Yet, analysis of a large-scale network is still challenging, given that many parameters need to be determined in advance. Estimation of all the parameters of a whole-cell model has not yet been appropriately resolved [6]. To analyze the dynamics of a large-scale network, it is often divided into feasible-size modules, which are defined as small networks of functional units amenable to simulation and analysis [7]. Overall, the bottom-up approach can be used to analyze part of a biological event around a source molecule, but it is not applicable to a large-scale network; the top-down approach cannot be applied to analyze the dynamics because of the problem of parameter estimation. A whole-cell mathematical model of the bacterium Mycoplasma genitalium, which contains 525 genes, was built on the basis of enormous experimental data [8]; however, the use of a life-cycle model is not a simple way to analyze the mechanisms of dynamic control and requires a lot of information about the particular species.

To comprehensively analyze the dynamics of regulatory mechanisms, we developed a hybrid method that combines the bottom-up and top-down approaches. We aimed to decrease the number of modeled elements without losing the characteristic dynamics; therefore, we focused on network motifs that are important for the dynamics. Network motifs are subgraph structures that recur more often in a metabolic network or gene regulation network than in a random network. They are important for determining intrinsic regulation mechanisms derived from network characteristics [9]. In the current method, we extracted motifs from a large-scale regulatory network and used them to reconstruct a simple network, which reflects the original dynamics of the entire network because it contains these important motifs. We especially focused on a cascade motif and a feed-back loop motif. A cascade motif is a sequence of unidirectional edges, and a feed-back loop is a circuit structure that feeds back some of the output to the input.

We then modeled the differentiation of neural stem cells (NSCs) and analyzed the characteristic changes of dynamics during differentiation. NSCs replicate and differentiate into neurons, astrocytes, or oligodendrocytes [10]. Some models simulate early differentiation or functional neurons [11, 12], but no model enables us to simulate and analyze the dynamics of the large-scale regulatory network of neuronal differentiation. The basic helix-loop-helix type transcription factors HES1, ASCL1, and OLIG2 show characteristic differences in their dynamics before and after differentiation [13]. They also maintain oscillatory dynamics during cell replication. If the concentration of ASCL1 is higher than that of HES1 during the non-oscillatory state, the NSCs differentiate into neurons. If the concentration of HES1 or OLIG2 is higher than that of ASCL1, the NSCs differentiate into astrocytes or oligodendrocytes, respectively [13]. In the current study, we constructed a comprehensive molecular-interaction network of NSC differentiation into neurons using the available data; we then developed a mathematical model that maintained the original dynamics of the network by integrating network motifs. The model could simulate the characteristic dynamic changes before and after differentiation. The model also reproduced the effect of overexpression or knockdown of the Id2 gene, which encodes an inhibitor of HES1 dimerization [14]. We suggest that stabilization of oscillations and characteristic dynamic changes are regulated by the combination of multiple feedback loops.

Figure 1 illustrates the analysis processes in this study. Our method allows the analysis of a comprehensive regulatory network by collecting information exhaustively and scaling down the network according to the rationality of dynamics without arbitrariness. On the basis of the analysis of the dynamics of neuronal differentiation, we here propose that a combination of multiple motifs is important to define the major dynamics of an entire network.
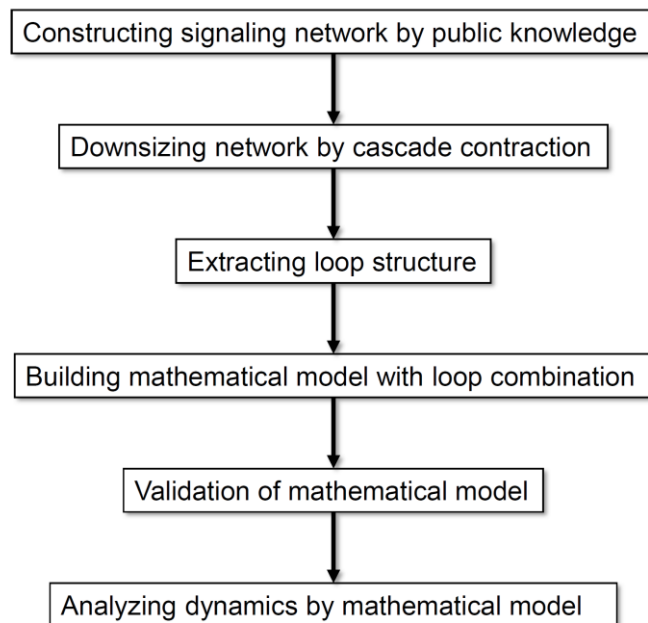
```
┌─────────────────────────────────────────────────┐
│  Constructing signaling network by public knowledge │
└─────────────────────────────────────────────────┘
                        │
                        ▼
┌─────────────────────────────────────────┐
│  Downsizing network by cascade contraction │
└─────────────────────────────────────────┘
                        │
                        ▼
          ┌──────────────────────────┐
          │  Extracting loop structure │
          └──────────────────────────┘
                        │
                        ▼
┌──────────────────────────────────────────────┐
│  Building mathematical model with loop combination │
└──────────────────────────────────────────────┘
                        │
                        ▼
      ┌───────────────────────────────────┐
      │  Validation of mathematical model  │
      └───────────────────────────────────┘
                        │
                        ▼
    ┌──────────────────────────────────────────┐
    │  Analyzing dynamics by mathematical model  │
    └──────────────────────────────────────────┘
```

Figure 1. Flow diagram of the analysis processes in this study.

2. Materials and Methods

2.1. Construction of a neuronal differentiation network

To construct the complete signaling network, relations among molecules involved in neuronal differentiation were collected from the literature and pathway databases [15–22], mainly the NCI Pathway Interaction Database [23] and WikiPathways [24]. Molecular interactions related to glial differentiation were excluded to focus on the differentiation of NSCs into neurons. The signaling networks were constructed using CellDesigner v4.3 [25] by merging binary relations from each data source and were saved in Systems Biology Markup Language (SBML) format. The complete signaling network was constructed by manually merging all the SBML files. Then, every molecule was color-coded according to its type (receptor, enzyme, transcription factor, or other). Finally, the enzymes and other molecules were divided into active and inactive forms. The graphical representation conformed to the proposed set of symbols in CellDesigner [26].

2.2. Contraction of the network

To simplify the network without losing the essential loop structures that are important to the original dynamics, the sequences of unidirectional edges (cascade motifs) were converted to a single edge between two molecules. The rate of a cascade reaction depends on the rate-limiting reaction; therefore, each cascade was represented as a single rate-limiting reaction. The contraction was continued manually until a network contained hub nodes only (or nearly so). After cascade contraction, feedback loop structures were extracted as a core network. At this time, a transcription–translation self-feedback loop, which was initially constructed from one or two molecules, was reconstructed to include three molecules by adding a transcription or translation event, because such events require much more time than signal transduction events, and this investment of time is related to nonlinear dynamics. Finally, to minimize the network size, feedback loops in the core network were contracted again until at least three nodes. After this contraction, the nodes of contracted cascade were named on the basis of the node name of the original cascade.

2.3. Mathematical model construction

The contracted network was converted into a mathematical model (digested model), in which the dynamics of the original network were maintained. The model was constructed using

CellDesigner. The contracted network was drawn and kinetics with parameters were assigned to every edge using the SBMLsqueezer [27] plug-in in CellDesigner. In SBMLsqueezer, the 'Reversibility' option was set to 'Use information from SBML'. Every type of enzyme kinetics was set to the Michaelis–Menten equation, which is one of the best-known models of enzyme kinetics. That of transcriptional or translational reactions was set to the Hill equation, which is the simplest way to describe sigmoidal responses. The parameters were estimated in the range of physiologically relevant values which could simulate the experimental results reported by Imayoshi et al. [13]. The range was determined from records in BioNumbers [28, 29]. The initial concentration of each protein was set to 1.0 μM because the typical concentration range of a signaling protein is 10 nM–1 μM [30]. For enzymes and other molecules, the concentration of the active and inactive form was set to 0.5 μM each.

2.4. Simulation and analysis

The dynamics of the digested model were validated by steady-state simulation and parameter analysis. Simulation was performed using CellDesigner, and the analysis was conducted using COPASI 4.14 (Build 89) [31]. The simulation was calculated using SOSlib [32] with the error tolerance set to −6. To simulate the change in dynamics due to the induction of differentiation, an event that perturbs the concentration of NOTCH (differentiation control factor) at an arbitrary time point was configured. The parameter search and bifurcation analysis were conducted using the Parameter Scan function in COPASI, which records the time course of an arbitrary molecule for 500-h while changing an arbitrary parameter or concentration within the defined range. The time course was calculated using LSODA [33] with the following parameters: Integrate Reduced Model, 0; Relative Tolerance, 1e–06; Absolute Tolerance, 1e–12; Max Internal Steps, 10,000. The scope of a parameter scan was set to 0.001–1000, and the range of NOTCH concentrations as a differentiation control factor was set to 0–2.8μM.

3. Results

3.1. Signaling network of neuronal differentiation

To construct a signaling network of NSC differentiation into a mature neuron, we collected publicly available information about the switch from NOTCH, a molecular marker of differentiation, to neuronal markers such as Tau. The network was constructed by using 54 molecules and contained five modules (Figure 2A). The first module was the differentiation switch from NOTCH. The second module was the expression of transcription factors that are early neural markers [15–19]. The third module was the transition from an immature neuron to a mature neuron. The fourth module was regulation to gain mature neuron functions [20, 21]. Finally, beta-catenin, a molecule related to the function of mature neurons, controls a bHLH-type transcription factor to adjust differentiation [22]. Converting this entire signaling network into a mathematical model can be challenging because multiple parameters need to be taken into account. Because the network dynamics are controlled by the dynamics of individual network motifs [34], we focused on feedback loop motifs that are important to nonlinear dynamics. For example, a feedback loop may confer the ability of homeostasis, ultra-sensitivity, hysteresis, and bistability [35]. A positive feedback loop is defined as a loop structure containing zero or an even number of negative regulations, and a negative feedback loop is defined as a loop structure containing an odd number of negative regulations (Figure 3A). Although some tools could find a loop structure [36, 37], it was difficult to find a large loop structure whose size is over 15 nodes. Therefore, to find a large loop, we need to extract a loop structure from complicated and large network manually. To facilitate manual extraction, we contracted the entire network by cascade contraction until a network contained hub nodes only, and extracted feedback loop motifs. (Figure 3B, Additional file 1: Figure S1 and Table S1). After contraction, feedback loop structures were extracted to obtain the core network of marker genes, which contained 14 molecules (Figure 2B). Although there were also

feed-forward loops in the entire network, they located on downstream of the network and had no connection to marker genes. So the feed-forward loop were omitted from core network. The core network included four feedback loop motifs: (1) a negative-feedback loop formed by HES1 dimerization, (2) a positive-feedback loop between PI3K and aPKC_PAR3_PAR6, (3) a negative-feedback loop between PTEN and GSK3B, and (4) a negative-feedback loop between beta-catenin and HES1. The first three loops have been previously investigated [16, 20] (the first one has been especially well analyzed [38, 39]), but the negative-feedback loop between beta-catenin and HES1, which was the largest in our model, has not been focused on. The core network retained the feedback loop motifs of the original entire network, and therefore was expected to maintain the original dynamics of marker molecules, HES1 and ASCL1. To analyze the dynamics of the core network, we constructed a mathematical model.
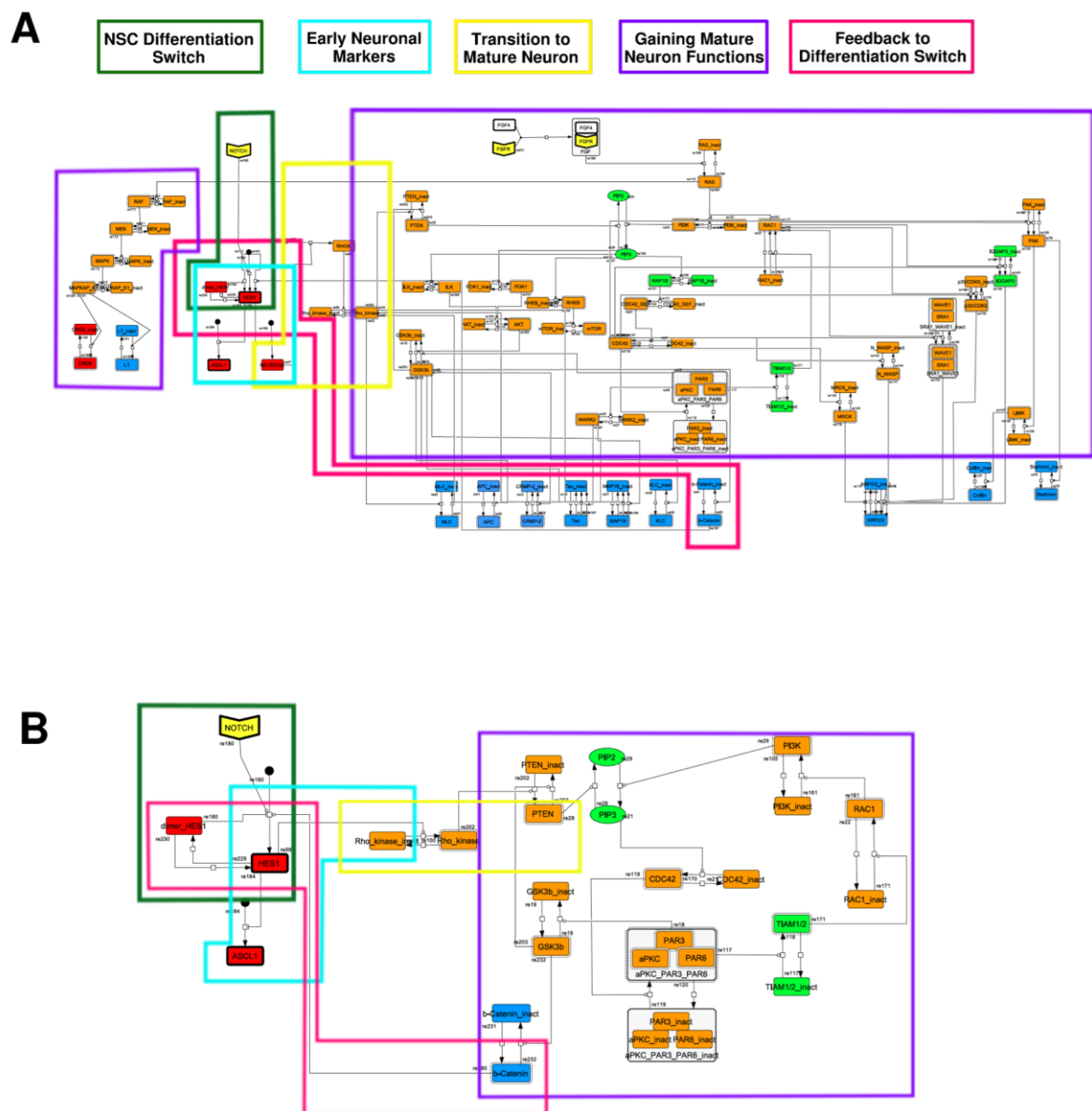
Figure 2. Signaling network of neural stem cell differentiation based on publicly available data. (A) The entire signaling network. (B) Core signaling network: feedback loops extracted from the entire network. Rectangle nodes are generic proteins. Oval nodes are small molecules. Arrowhead node is receptor. Dashed-line nodes are active forms. Bold-line nodes are neuronal markers. Node color codes: yellow, receptor; red, transcription factor; orange, enzyme; blue, molecule related to a function of mature neuron; green, other.
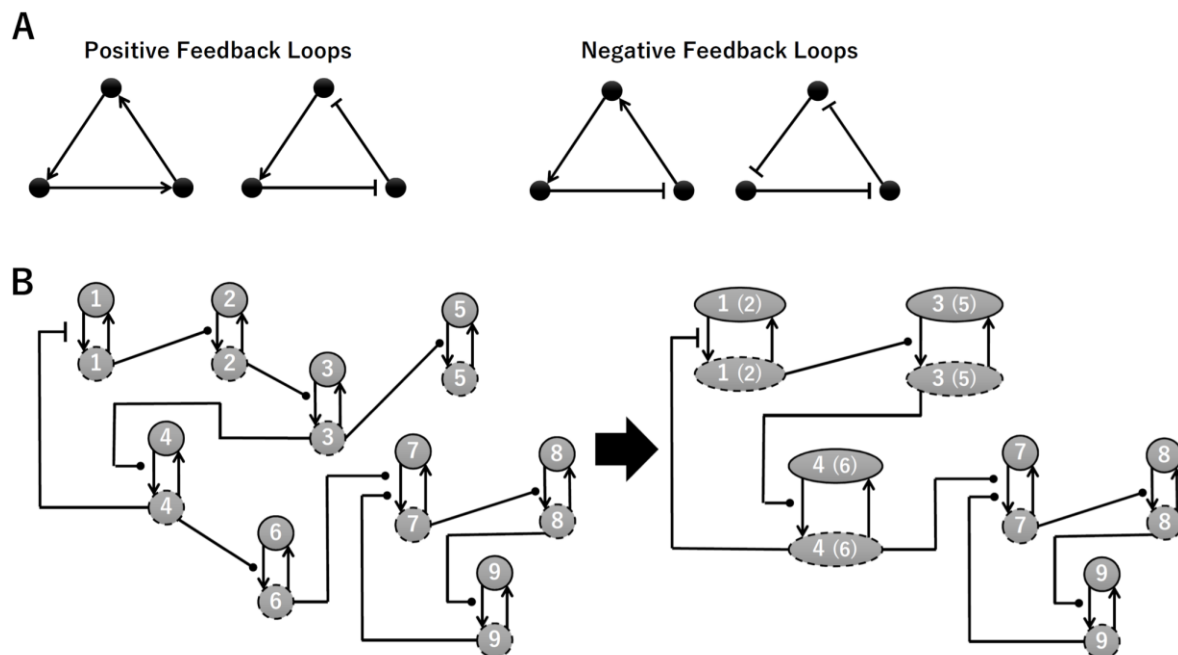
Figure 3. Feedback loops and contraction. (A) Examples of positive and negative feedback loops. (B) Example of contraction.

3.2. Mathematical model of the core network

Because the core network was still too complex to convert into a mathematical model, we contracted it to the minimum nodes but maintained the feedback loop structures, including the differentiation switch NOTCH and the indicators of characteristic dynamics before and after differentiation (Figure 4, Additional file 3). The self-negative-feedback loop formed by HES1 dimerization was reconstructed as a three-molecule loop by adding mRNA of HES1 (mHES1) as a transcriptional process, because the self-negative feedback loop represented by transcriptional and translational processes was actually composed of the generation of mRNA and translation of the mRNA (see Methods for details). Although previous studies introduced a delay into the model [11, 12], we convolved the delay with the parameters of the HES1 translation and dimerization steps. The non-delay model of the HES1 self-loop generated oscillations (Additional file 1: Figures S2, S3, and Table S2). To minimize the network, most feedback loops were converted to three-molecule loops by cascade contraction. The contracted cascades were represented with the nodes in our digested model. The names of the nodes were determined based on the name of the first or the last node of the original cascade with the addition of the suffix _ca or _ci. The suffix _ca denoted the active form of a cascade, and _ci denoted the inactive form. The positive-feedback loop between PI3K and aPKC_PAR3_PAR6 was reconstructed as a three-molecule loop, and the contracted nodes were named PIP_ca (PIP_ci), aPKC_ca (aPKC_ci), and PI3K_ca (PI3K_ci) (Additional file 1: Figure S4). The negative-feedback loop between PTEN and GSK3B was reconstructed as a four-molecule loop, and the contracted nodes were named PTEN_ca (PTEN_ci) and GSK3B_ca (GSK3B_ci) (Additional file 1: Figure S5). The negative-feedback loop between beta-catenin and HES1 was reconstructed as a six-molecule loop (Additional file 1: Figure S6). This network translated into a deterministic mathematical digestedmodel governed by the Hill equation and Michaelis–Menten kinetics (Table 1). The final digestedmodel was constructed using 9 molecules (16 nodes) and 20 reactions, which reduced the network size by 84.3% in comparison with the entire signaling

network. Thereafter, the dynamics of neuronal differentiation were analyzed by using the digestedmodel.
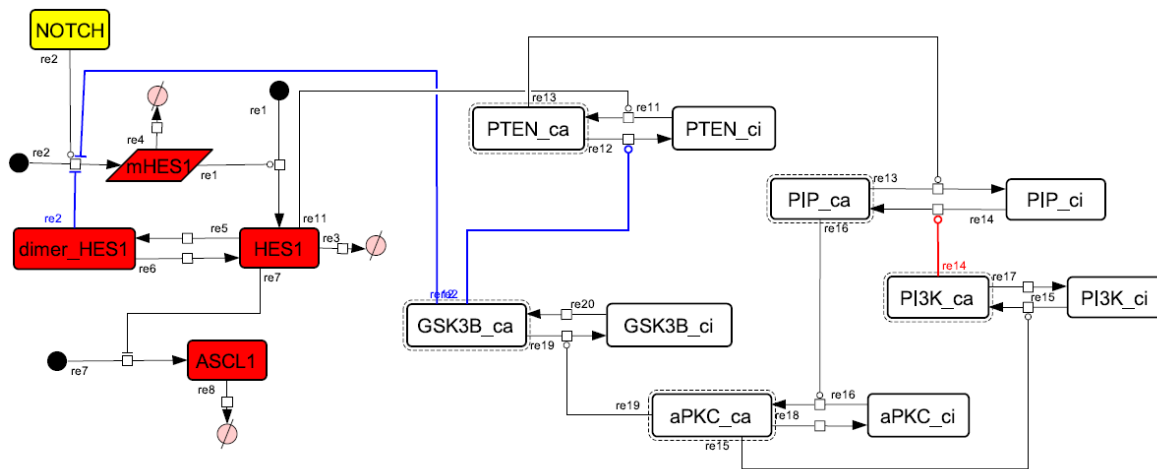

Figure 4. Diagram of the toy model. The model consists of multiple feedback loops extracted from the core signaling network. Red edge is a component of a positive feedback loop. Blue edges are components of negative feedback loops. Node color codes: yellow, receptor; red, transcription factor; white, contracted node.

Table 1. Differential equations of the toy model.

Equation No.	Equation
1	$$\frac{d[\mathrm{HES1}]}{dt} = kg_2 \cdot [\mathrm{mHES1}] - k_{s3_d} \cdot [HES1] - 2 \cdot k_3 \cdot [HES1]^2 + 2 \cdot k_{3r} \cdot [dimer_{HES1}]$$
2	$$\frac{d[\mathrm{mHES1}]}{dt} = \frac{kg_1 \cdot [NOTCH]^{np_{re2_{s11}}}}{[NOTCH]^{np_{re2_{s11}}} + kSp_{re2_{s11}}^{np_{re2_{s11}}}} \cdot \left(1 - \frac{[dimer_{HES1}]^{np_{re2_{s9}}}}{[dimer_{HES1}]^{np_{re2_{s9}}} + kSm_{re2_{s9}}^{np_{re2_{s9}}}}\right)$$ $$\cdot \left(1 - \frac{[GSK3B_{ca}]^{np_{re2_{s24}}}}{[GSK3B_{ca}]^{np_{re2_{s24}}} + kSm_{re2_{s24}}^{np_{re2_{s24}}}}\right) - k_{s2_d}[mHES1]$$
3	$$\frac{d[dimer_{HES1}]}{dt} = k_3 \cdot [HES1]^2 - k_{3r} \cdot [dimer_{HES1}]$$
4	$$\frac{d[ASCL1]}{dt} = kg_{re7} \cdot \left(1 - \frac{[HES1]^{nm_{re7_{s3}}}}{[HES1]^{nm_{re7_{s3}}} + kSm_{re7_{s3}}^{nm_{re7_{s3}}}}\right) - kass_{re8} \cdot [ASCL1]$$
5	$$\frac{d[PTEN_{ca}]}{dt} = \frac{[HES1] \cdot kcatp_{re11} \cdot [PTEN_{ci}]}{kM_{re11_{s15}} + [PTEN_{ci}]} - \frac{[GSK3B_{ca}] \cdot kcatp_{re12} \cdot [PTEN_{ca}]}{kM_{re12_{s22}} + [PTEN_{ca}]}$$
6	$$\frac{d[PTEN_{ci}]}{dt} = \frac{[GSK3B_{ca}] \cdot kcatp_{re12} \cdot [PTEN_{ca}]}{kM_{re12_{s22}} + [PTEN_{ca}]} - \frac{[HES1] \cdot kcatp_{re11} \cdot [PTEN_{ci}]}{kM_{re11_{s15}} + [PTEN_{ci}]}$$
7	$$\frac{d[PIP_{ca}]}{dt} = \frac{[PI3K_{ca}] \cdot kcatp_{re14} \cdot [PIP_{ci}]}{kM_{re14_{s17}} + [PIP_{ci}]} - \frac{[PTEN_{ca}] \cdot kcatp_{re13} \cdot [PIP_{ca}]}{kM_{re13_{s16}} + [PIP_{ca}]}$$

8
$$\frac{d[PIP_{ci}]}{dt} = \frac{[PTEN_{ca}] \cdot kcatp_{re13} \cdot [PIP_{ca}]}{kM_{re13_{s16}} + [PIP_{ca}]} - \frac{[PI3K_{ca}] \cdot kcatp_{re14} \cdot [PIP_{ci}]}{kM_{re14_{s17}} + [PIP_{ci}]}$$

9
$$\frac{d[PI3K_{ca}]}{dt} = \frac{[aPKC_{ca}] \cdot kcatp_{re15} \cdot [PI3K_{ci}]}{kM_{re15_{s21}} + [PI3K_{ci}]} - \frac{Vp_{re17} \cdot [PI3K_{ca}]}{kM_{re17_{s20}} + [PI3K_{ca}]}$$

10
$$\frac{d[PI3K_{ci}]}{dt} = \frac{Vp_{re17} \cdot [PI3K_{ca}]}{kM_{re17_{s20}} + [PI3K_{ca}]} - \frac{[aPKC_{ca}] \cdot kcatp_{re15} \cdot [PI3K_{ci}]}{kM_{re15_{s21}} + [PI3K_{ci}]}$$

11
$$\frac{d[aPKC_{ca}]}{dt} = \frac{[PIP_{ca}] \cdot kcatp_{re16} \cdot [aPKC_{ci}]}{kM_{re16_{s19}} + [aPKC_{ci}]} - \frac{Vp_{re18} \cdot [aPKC_{ca}]}{kM_{re18_{s18}} + [aPKC_{ca}]}$$

12
$$\frac{d[aPKC_{ci}]}{dt} = \frac{Vp_{re18} \cdot [aPKC_{ca}]}{kM_{re18_{s18}} + [aPKC_{ca}]} - \frac{[PIP_{ca}] \cdot kcatp_{re16} \cdot [aPKC_{ci}]}{kM_{re16_{s19}} + [aPKC_{ci}]}$$

13
$$\frac{d[GSK3B_{ca}]}{dt} = \frac{Vp_{re20} \cdot [GSK3B_{ci}]}{kM_{re20_{s22}} + [GSK3B_{ci}]} - \frac{[aPKC_{ca}] \cdot kcatp_{re19} \cdot [GSK3B_{ca}]}{kM_{re19_{s24}} + [GSK3B_{ca}]}$$

14
$$\frac{d[GSK3B_{ci}]}{dt} = \frac{[aPKC_{ca}] \cdot kcatp_{re19} \cdot [GSK3B_{ca}]}{kM_{re19_{s24}} + [GSK3B_{ca}]} - \frac{Vp_{re20} \cdot [GSK3B_{ci}]}{kM_{re20_{s22}} + [GSK3B_{ci}]}$$

3.3. Simulation of the oscillatory dynamics

To simulate the oscillatory state of HES1 and ASCL1 in undifferentiated NSCs as a basal condition (as reported by Imayoshi et al. [13]), the digestedmodel was investigated using an oscillatory parameter set. The ranges of 40 parameters (Table 2) allowed the model to maintain oscillations. To check whether these parameter values were physiologically relevant, we compared them to the general parameter values of Michaelis–Menten kinetics based on the BioNumbers database [28]. The minimal values of the parameters in Hill equation that allowed to reconstruct the expected behaviors of the model were chosen. Almost all parameters of enzymes, except kM_re2_s24 and kM_re2_s9, exhibit KM values above 0.1 μM [29], and almost all of the KM values in the model were above 0.1 μM in the oscillatory range. The maximum (37,596,000 h−1) and minimum (264 h−1) Kcat values were acquired from 27 records for mammals in BioNumbers (Additional File 2); all Kcat values in the model were within this range. These data indicated that the oscillatory state could be established under physiologically relevant conditions. The model could simulate the HES1 and ASCL1 oscillation within the 2.5-h period reported by Imayoshi et al. [13] in the undifferentiated state as the basal condition (Figure 5A, Additional file 1: Figure S7).

Table 2. Oscillation parameter ranges.

Parameter (unit)	2.5-h period	Minimum	Maximum	Parameter description
k_{s2_d} (h^{-1})	0.99	0.69	2.45	Degradation rate constant of reaction 3 for substrate s3
k_{S3_d} (h^{-1})	1.29	1.03	2.28	Degradation rate constant of reaction 4 for substrate s2
k_3 (μM·h^{-1})	0.4074	0.37	0.65	Dimerization rate constant of reaction 5
k_{3r} (h^{-1})	2.3	0.61	2.49	Dissociation rate constant of reaction 6
$kass_{re8}$ (h^{-1})	31.2	<0.001	>100	Degradation rate constant of reaction 8 for substrate s5
$kcatp_{re11}$ (h^{-1})	141.6	108	146	Turnover number of reaction 11
$kcatp_{re12}$ (h^{-1})	132.6	130	174	Turnover number of reaction 12
$kcatp_{re13}$ (h^{-1})	209.4	162	216	Turnover number of reaction 13
$kcatp_{re14}$ (h^{-1})	132	128	173	Turnover number of reaction 14
$kcatp_{re15}$ (h^{-1})	132	128	173	Turnover number of reaction 15
$kcatp_{re16}$ (h^{-1})	174	171	238	Turnover number of reaction 16
$kcatp_{re19}$ (h^{-1})	132	95	183	Turnover number of reaction 19
kg_1 (μM·h^{-1})	361.2	183	526	Maximal transcription rate of reaction 2
kg_2 (μM·h^{-1})	25.74	13.1	31.6	Mass action constant of reaction 1
kg_{re7} (μM·h^{-1})	10.86	<0.001	>100	Maximal transcription rate of reaction 7

$kM_{re11_{s15}}$ (µM)	50.0	48.9	65.5	Michaelis–Menten constant of reaction 11 for substrate s15
$kM_{re12_{s22}}$ (µM)	1.62	1.26	1.66	Michaelis–Menten constant of reaction 12 for substrate s22
$kM_{re13_{s16}}$ (µM)	0.21	0.21	0.29	Michaelis–Menten constant of reaction 13 for substrate s16
$kM_{re14_{s17}}$ (µM)	28.4	21.6	28.9	Michaelis–Menten constant of reaction 14 for substrate s17
$kM_{re15_{s21}}$ (µM)	12.7	9.4	13.1	Michaelis–Menten constant of reaction 15 for substrate s21
$kM_{re16_{s19}}$ (µM)	0.45	0.22	0.49	Michaelis–Menten constant of reaction 16 for substrate s19
$kM_{re17_{s20}}$ (µM)	1.2	1.18	1.61	Michaelis–Menten constant of reaction 17 for substrate s20
$kM_{re18_{s18}}$ (µM)	0.91	0.89	1.52	Michaelis–Menten constant of reaction 18 for substrate s18
$kM_{re19_{s24}}$ (µM)	9.0	6.2	12.8	Michaelis–Menten constant of reaction 19 for substrate s24
$kM_{re20_{s23}}$ (µM)	0.62	0.38	0.88	Michaelis–Menten constant of reaction 20 for substrate s23
$kSm_{re2_{s24}}$ (µM)	0.04	0.029	0.048	Half-maximal inhibitory concentration of substrate s24 in reaction 2
$kSm_{re2_{s9}}$ (µM)	0.0023	<0.001	0.0025	Half-maximal inhibitory concentration of substrate s9 in reaction 2
$kSm_{re7_{s3}}$ (µM)	0.116	<0.001	>100	Half-maximal inhibitory concentration of substrate s3 in reaction 7

$kSp_{re2_{s11}}$ (µM)	2.5	2.18	3.17	Half-maximal effective concentration of substrate s24 in reaction 2
Vp_{re17} (µM·h^{-1})	88.2	67.9	90.9	Maximal reaction rate constant of reaction 17
Vp_{re18} (µM·h^{-1})	14.52	10.7	14.9	Maximal reaction rate constant of reaction 18
Vp_{re20} (µM·h^{-1})	24.0	17.9	33.3	Maximal reaction rate constant of reaction 20
$nm_{re2_{s24}}$	2	2	2	Inhibition coefficient of reaction 2 for substrate s24
$nm_{re2_{s9}}$	5	5	>10	Inhibition coefficient of reaction 2 for substrate s9
$nm_{re7_{s3}}$	2	1	>10	Inhibition coefficient of reaction 7 for substrate s3
$np_{re2_{s11}}$	3	2	3	Hill coefficient of reaction 2 for substrate s11
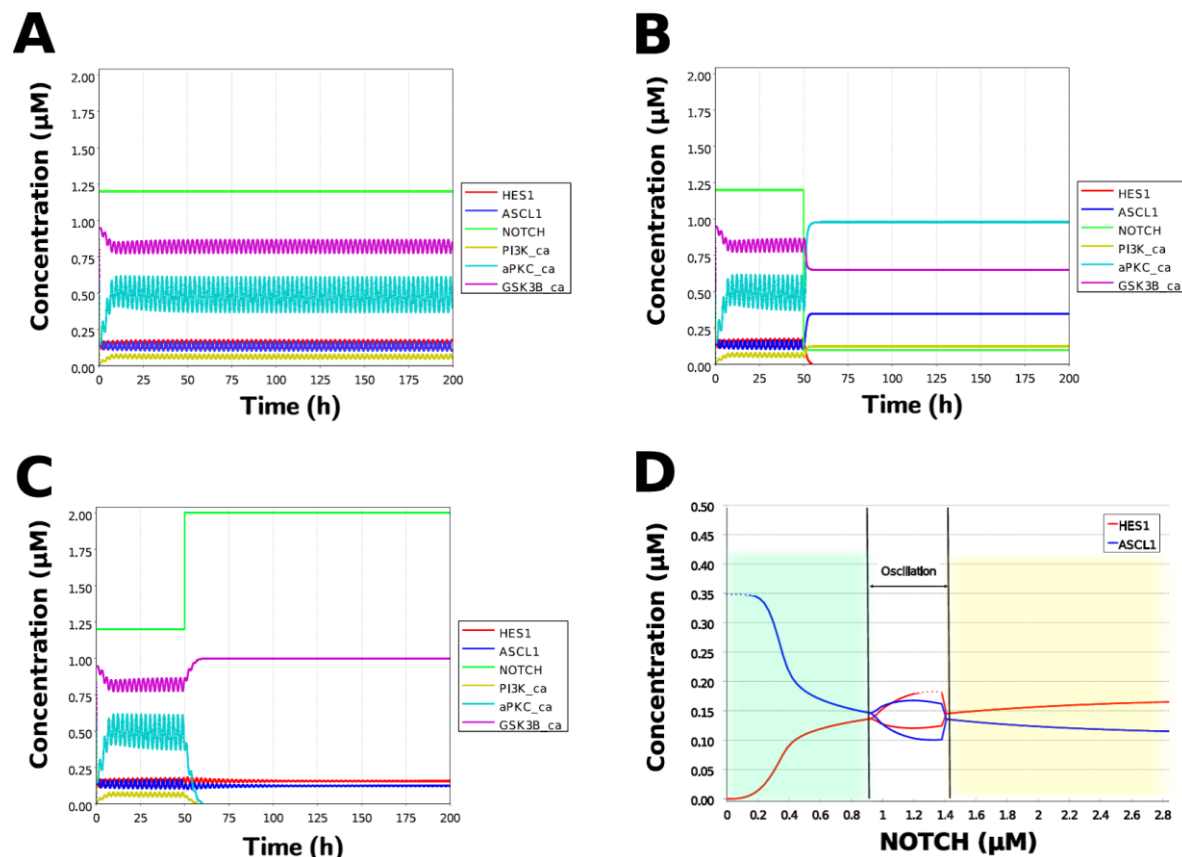
Figure 5. Simulation of the toy model. (A) Basic condition with a 2.5-h period. (B) Negative and (C) positive perturbation of NOTCH concentration at 50 h. (D) Bifurcation analysis of HES1 and ASCL1 concentrations dependence on NOTCH concentration. Background colors show cell differentiation state; green, neuron; yellow, astrocyte.

3.4. Model validation

During neural differentiation, the characteristic dynamics of the transition from the oscillatory to the non-oscillatory state of HES1 and ASCL1 are controlled by the concentration of NOTCH [13]. In the non-oscillatory state after differentiation, the concentration of ASCL1 was higher than that of HES1 in a neuron, whereas the concentration of HES1 was higher than that of ASCL1 in an astrocyte. To simulate the physiological condition at the initiation of neuronal differentiation, we set a low concentration of NOTCH during simulation. As a result, ASCL1 became dominant in a non-oscillatory state. At the same time, the concentration of GSK3B_ca, which included GSK3B (a negative regulator [20]), decreased and the concentrations of aPKC_ca, which included aPKC_PAR3_PAR6, and PI3K_ca, which included PI3K (positive regulators [20]), increased (Figure 5B). These results agreed with the previously reported experimental results during neuronal differentiation [13, 20]. Conversely, we set a high concentration of NOTCH and executed simulation. The oscillation of the concentrations of HES1 and ASCL1 disappeared and the equilibrium concentration of HES1 became higher than that of ASCL1 (Figure 5C). This result agrees with the previously reported initiation of glial differentiation [13]. Both ASCL1 and HES1 maintained oscillations at physiologically relevant NOTCH concentrations in an NSC (Figure 5D) [30]. This NOTCH-dependent dynamic transition was consistent with the experimental results of Imayoshi et al. [13].

We also simulated the overexpression and knockdown of the Id2 gene, which encodes an inhibitor of HES1 dimerization [14]. The knockdown of Id2 promotes neuronal differentiation by suppressing HES1 and enhancing ASCL1 expression, and the overexpression of Id2 inhibits neuronal differentiation by enhancing HES1 and suppressing ASCL1 expression [14]. To simulate the inhibition of HES1 dimerization by Id2, an inhibition parameter, kSm_Id (an indicator of the

amount of Id2), was introduced into equations 1 and 3 (Table 1) to obtain equations 1' and 3' (Table 3), respectively. When Id2 knockdown was simulated by setting kSm_Id to 0.1, oscillations disappeared, and a neuronal differentiation state with ASCL1 domination was observed at each NOTCH concentration (Figure 6A). When Id2 overexpression was simulated by setting kSm_Id to 10, oscillations also disappeared, and a non-neuronal differentiation state with HES1 domination was observed at NOTCH concentrations over 0.7 μM (Figure 6B). Thus, the digestedmodel maintained the original dynamics of the entire network.

A

B
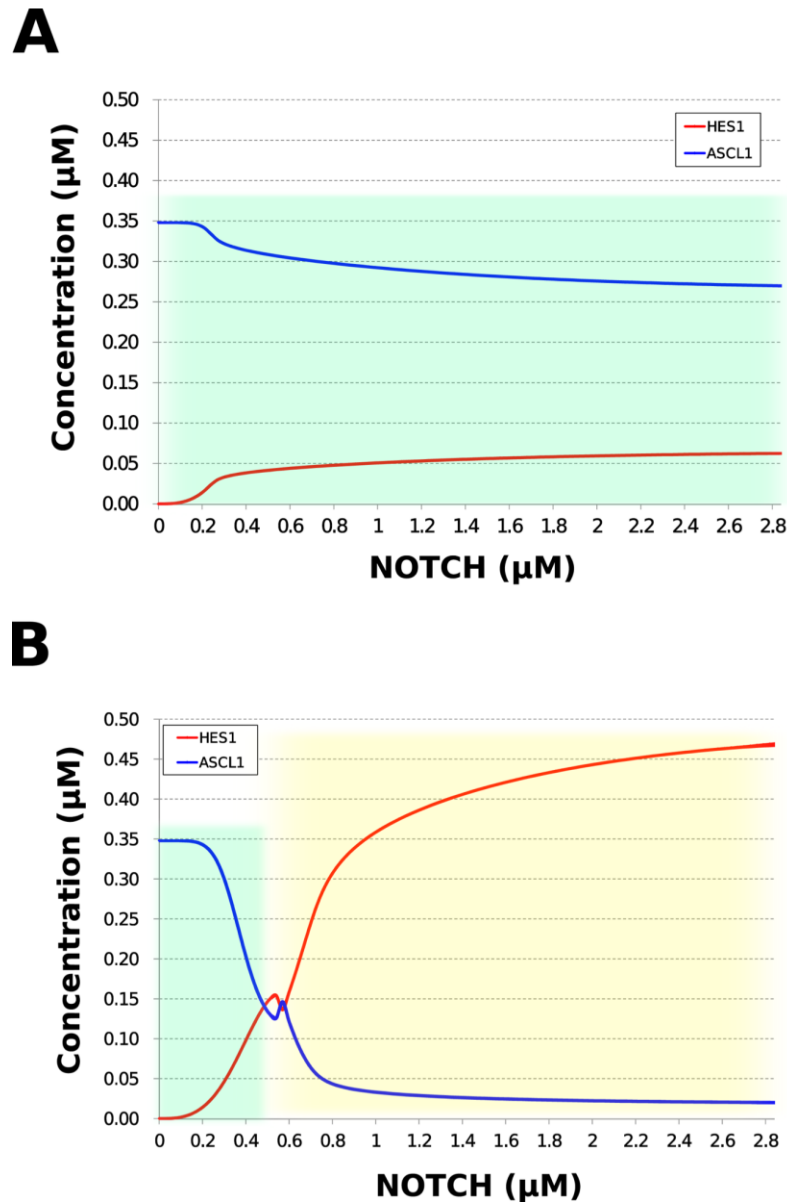
Figure 6. Simulation of HES1 and ASCL1 concentrations under the Id2 gene knockdown or overexpression conditions. (A) Id2 gene knockdown with kSm_Id = 0.1. (B) Id2 gene overexpression with kSm_Id = 10. Background colors show cell differentiation state; green, neuron; yellow, astrocyte.

Table 3. Differential equations of a model with incorporated inhibition of HES1 dimerization by Id2.

Equation No.	Equation
1'	$\dfrac{d[\text{HES1}]}{dt} = kg_2 \cdot [\text{mHES1}] - k_{s3_d} \cdot [\text{HES1}] - \dfrac{2 \cdot k_3 \cdot [\text{HES1}]^2}{kSm_{Id}} + 2 \cdot k_{3r} \cdot [dimer_{HES1}]$
3'	$\dfrac{d[dimer_{HES1}]}{dt} = \dfrac{k_3 \cdot [\text{HES1}]^2}{kSm_{Id}} - k_{3r} \cdot [dimer_{HES1}]$

3.5. Network motif analysis

We analyzed the contribution of each motif to the results of simulation of NOTCH responsiveness by bifurcation analysis. To simulate a loss-of-function mutation that inhibits the self-feedback regulation of HES1, we collapsed the self-feedback loop of HES1 in our model and executed simulation. When the loop was collapsed by changing equation 2 to equation 2' (Table 4), the oscillatory state, which is important for maintaining the undifferentiated state, disappeared (Figure 7A). This result was consistent with the reported importance of the HES1 self-feedback loop in neuronal differentiation [38, 39]. To simulate the specific inhibition of the effect of GSK3B on PTEN, we collapsed the negative feedback loop between GSK3B and PTEN by changing equations 5 and 6 to equations 5' and 6', respectively (Table 4). The oscillatory state shifted to higher NOTCH concentrations (Figure 7B), which means that this loop was involved in the sensitivity of oscillations to NOTCH concentration. GSK3B may promote or inhibit NOTCH signaling under different conditions depending on the loops involved [40-43]. The dichotomic characteristics of GSK3B may enable it to arbitrate the response to NOTCH, given that our simulation suggested that the GSK3B–PTEN loop regulated the sensitivity of oscillations to NOTCH. To simulate the specific inhibition of the effect of PI3K to PIP2, we collapsed the positive feedback loop between aPKC_PAR3_PAR6 and PI3K by changing equations 7 and 8 to equations 7' and 8', respectively (Table 4). The relative changes in HES1 and ASCL1 concentrations with NOTCH concentration were maintained, but the oscillatory state disappeared (Figure 7C); therefore, the aPKC_PAR3_PAR6–PI3K loop is required to maintain the oscillatory state. We estimated the effect of the collapse of this loop by inhibiting PI3K. A PI3K inhibitor, LY294002, inhibits proliferation of neural progenitor cells [22, 43]; our result agreed with the published data. To simulate the specific inhibition of the effect of beta-catenin on HES1, we collapsed the negative feedback loop between beta-catenin and HES1 by changing equation 2 to equation 2'' (Table 4). The oscillations disappeared, and the ASCL1-dominant state became narrower (Figure 7D), indicating that this loop is required for maintaining oscillations and upregulating ASCL1 at low concentrations of NOTCH. The collapse of this loop equals beta-catenin inhibition, which represses proliferation of neural progenitor cells and accelerates glial differentiation [44, 45]. Glial differentiation is induced without oscillation under ASCL1 repression [13]. Our result that the collapse of this loop leads to ASCL1 repression is consistent with the reported acceleration of glial differentiation by beta-catenin inhibition. These results suggest that multiple feedback loops are essential for the characteristic dynamics of neural differentiation.
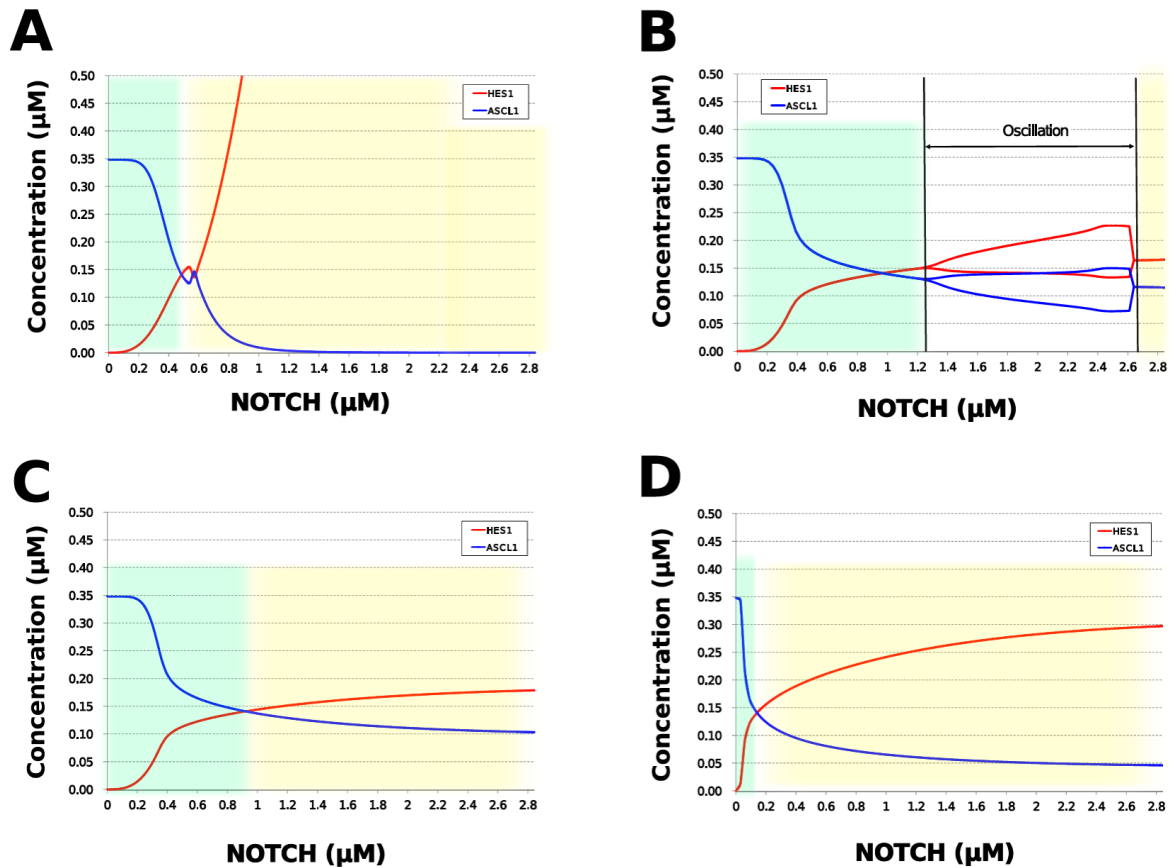
Figure 7. Bifurcation analysis of HES1 and ASCL1 concentration dependence on NOTCH concentration when each feedback loop is collapsed. (A) Collapsed HES1 self-feedback loop. (B) Collapsed negative-feedback loop between GSK3B and PTEN. (C) Collapsed positive-feedback loop between aPKC_PAR3_PAR6 and PI3K. (D) Collapsed negative-feedback loop between beta-catenin and HES1. Background colors show cell differentiation state; green, neuron; yellow, astrocyte.

Table 4. Differential equations of models with feedback loop removed.

Equation No.	Equation
2'	$$\frac{d[mHES1]}{dt} = \frac{kg_1 \cdot [NOTCH]^{np_{re2_{S11}}}}{[NOTCH]^{np_{re2_{S11}}} + kSp_{re2_{S11}}^{np_{re2_{S11}}}} \cdot 1$$ $$\cdot \left(1 - \frac{[GSK3B_{ca}]^{np_{re2_{S24}}}}{[GSK3B_{ca}]^{np_{re2_{S24}}} + kSm_{re2_{S24}}^{np_{re2_{S24}}}}\right) - k_{s2_d}[mHES1]$$
2''	$$\frac{d[mHES1]}{dt} = \frac{kg_1 \cdot [NOTCH]^{np_{re2_{S11}}}}{[NOTCH]^{np_{re2_{S11}}} + kSp_{re2_{S11}}^{np_{re2_{S11}}}} \cdot \left(1 - \frac{[dimer_{HES1}]^{np_{re2_{S9}}}}{[dimer_{HES1}]^{np_{re2_{S9}}} + kSm_{re2_{S9}}^{np_{re2_{S9}}}}\right)$$ $$\cdot 1 - k_{s2_d}[mHES1]$$
5'	$$\frac{d[PTEN_{ca}]}{dt} = \frac{[HES1] \cdot kcatp_{re11} \cdot [PTEN_{ci}]}{kM_{re11_{S15}} + [PTEN_{ci}]} - \frac{1 \cdot kcatp_{re12} \cdot [PTEN_{ca}]}{kM_{re12_{S22}} + [PTEN_{ca}]}$$

6' $$\frac{d[PTEN_{ci}]}{dt} = \frac{1 \cdot kcatp_{re12} \cdot [PTEN_{ca}]}{kM_{re12_{s22}} + [PTEN_{ca}]} - \frac{[HES1] \cdot kcatp_{re11} \cdot [PTEN_{ci}]}{kM_{re11_{s15}} + [PTEN_{ci}]}$$

7' $$\frac{d[PIP_{ca}]}{dt} = \frac{1 \cdot kcatp_{re14} \cdot [PIP_{ci}]}{kM_{re14_{s17}} + [PIP_{ci}]} - \frac{[PIP_{ca}] \cdot kcatp_{re13} \cdot [PIP_{ca}]}{kM_{re13_{s16}} + [PIP_{ca}]}$$

8' $$\frac{d[PIP_{ci}]}{dt} = \frac{[PTEN_{ca}] \cdot kcatp_{re13} \cdot [PIP_{ca}]}{kM_{re13_{s16}} + [PIP_{ca}]} - \frac{1 \cdot kcatp_{re14} \cdot [PIP_{ci}]}{kM_{re14_{s17}} + [PIP_{ci}]}$$

4. Discussion

We generated an NSC differentiation network containing four feedback loops on the basis of publicly available data. Our digested model was constructed through cascade contraction of the comprehensive regulatory network with preservation of feedback loops. Three types of HES1 and ASCL1 states regulated by NOTCH concentration were consistent with NOTCH-dependent neural differentiation suggested by Imayoshi et al. [13]. Although experimental data show complex waveforms of HES1 and ASCL1, we simulated the main-frequency waves, which have a period of 2 to 3 h [13], and analyzed the dynamics of the transition from the oscillatory to the non-oscillatory state qualitatively using a digested model. The results of the simulation of GSK3B, aPKC_PAR3_PAR6, and PI3K, represented as GSK3B_ca, aPKC_ca, and PI3K_ca in the digested model respectively, are consistent with previous experimental results [20] (Figure 5B, C). The results of the simulation of Id2 knockdown or overexpression are also consistent with experimental results [14]. Therefore, our digested model could adequately simulate the dynamics not only of HES1 and ASCL1 but also of other molecules. Our model suggests that three loops (HES1 negative self-feedback, positive feedback between aPKC_PAR3_PAR6 and PI3K, and negative feedback between GSK3B and HES1) are important to maintain undifferentiated state oscillations. We suggest that the negative-feedback loop between beta-catenin and HES1 in the comprehensive regulatory network is most important because of its greatest contribution to the characteristic dynamics (Figure 7D). A relation between beta-catenin and HES1 plays a role in tumorigenesis [46]. As HES1 controls cancer stem cells [47], the negative feedback loop that has not been focused on may be related to proliferation and differentiation of cancer stem cells. It is expected that a further experimental study such as making perturbation to the loop by knock down will reveal detail mechanism of neural differentiation. These findings could only be made by using the analysis based on a large-scale regulatory network, thus highlighting the effectiveness of our approach.

We demonstrated that focusing on feedback loop motifs instead of the whole network when constructing a model was sufficient for agreement with experimental results. Our approach could be applied to analysis of various biochemical networks by simulation. By streamlining large-scale regulatory network construction, our approach could help to analyze various biological phenomena, such as cell differentiation, cell division, or pathogenesis. However, the large-scale regulatory network will be probably insufficient and heterogeneous when it is constructed using the available data alone. To overcome this false-negative problem (the relations that exist but cannot be detected), many data-driven network reconstruction methods have been developed. These statistical approaches are mainly classified under two categories, expression based [48] and sequence based [49]. Although the methods of both categories could reveal undiscovered relations that could not be inferred manually, the reconstructed network includes many false-positive regulations. A nonlinear model intrinsically causes a complex behavior. With an increase in the number of false-positive regulations, an increase in the number of nonlinearities becomes avoidable. Based on this mathematical background, a model with a high number of false-positive

regulations seemingly generates the real behavior, but is different from the real system; therefore, it is desirable to build a mathematical model only from reliable elements. Addition of false-positive regulation to the model could have a considerable effect and complicate the conversion of a data-driven network into a mathematical model. Currently, the manual methods are better than the data-driven methods for construction of a mathematical model.

Our large-scale regulatory network of neuronal differentiation may lack some components and thus may not completely represent neuronal differentiation. In our network, ASCL1 is directly affected by HES1; ASCL1 oscillation controls proliferation and differentiation [13] and affects NOTCH receptors of adjacent cells via activation of DLL [50]. Neural differentiation is also affected by adjacent cells [51]. We excluded this information because we focused on the dynamics of a single cell. To reveal the entire mechanism of neural differentiation, adding a path to adjacent cells, for instance via DLL, might be required. The analysis of multiple cells might provide a model that can simulate dynamics other than state transitions. The concentrations of both HES1 and ASCL1 decrease in a non-oscillatory state when an NSC differentiates into an oligodendrocyte [13]. To simulate this transition, we need to add a signaling pathway focusing on the oligodendrocyte marker OLIG2, which oscillates with a period of 400 min in NSCs [13]. This period is much longer than that of HES1 or ASCL1, and the dispersion of the oscillation is very high; therefore, OLIG2 regulation might involve a delay mechanism to elongate the period and a mechanism to amplify dispersion. Recently, a similar method was used to analyze oligodendrocyte differentiation [52]. Similar to our study, the authors used a manual method to construct a network; however, they also introduced publicly available interaction data from omics databases. In comparison with our method, this approach may reduce the number of false-negative interactions. On the other hand, the study [52] focused only on two- to four-node feedback loops. Our contraction method may detect a larger regulatory system of oligodendrocyte differentiation. The complete mechanism of neural differentiation may be simulated by integrating this information and methods.

Our model can simulate the dynamics of the NSC-to-neuron transition and exemplify the reverse transition by increasing the concentration of NOTCH, but differentiation is mostly irreversible. Therefore, it is difficult to validate the results of reversing from a neuron to an NSC. Some hypotheses suggest the core factors of differentiation that also inhibit reprogramming [53] or control the mechanisms generated by neurogenic niches [54]. Specific network structure such as positive feedbacks or micro-environmental factors may be important for hysteresis in differentiation, and a more detailed, larger network needs to be analyzed. Although we focused on NOTCH signaling in this study, our network also includes FGF as another input signal. Analysis of the behavior of the network stimulated with FGF may show variate responses and as a result may reveal other mechanisms of neural differentiation. A feed-forward loop accelerates response time of a system and achive cell state transition rapidly. Because the cellular state transition by NOTCH signaling is also known to be accelerated by feed-forward loop [55], a feed-forward loop may exist on upstream of our analyzing network. Our method can be used to analyze the dynamics of a new large-scale regulatory network when new information becomes available.

5. Conclusions

The construction of a large-scale regulatory regulatory network of neuronal differentiation based on publicly available data led to identification of a new feedback loop motif, which we expect to regulate differentiation. The large-scale regulatory regulatory network was modeled mathematically after network contraction, and the extracted digested model simulated the characteristic dynamics of HES1 and ASCL1, which were suggested to be regulated by multiple loops. More information about neural differentiation and further motif analyses will deepen our understanding of the mechanism of neural differentiation. Our approach is applicable to other biological models for which detailed mechanisms are unknown.

Supplementary Materials: The following are available online at www.mdpi.com/xxx/s1, Figure S1: title, Table S1: title, Video S1: title.

References

1. Bruggeman FJ; Westerhoff HV. The nature of systems biology. *Trends Microbiol.* **2007**, *15(1)*, 45–50.
2. Chen KC; Calzone L; Csikasz-Nagy A; Cross FR; Novak B; Tyson JJ. Integrative analysis of cell cycle control in budding yeast. *Mol Biol Cell.* **2004**, *15(8)*, 3841–62.
3. Vignes M; Vandel J; Allouche D; Ramadan-Alban N; Cierco-Ayrolles C; Schiex T; Mangin B; de Givry S. Gene regulatory network reconstruction using Bayesian networks, the Dantzig Selector, the Lasso and their meta-analysis. *PLoS One.* **2011**, *6(12)*, e29165.
4. Chai LE; Loh SK; Low ST; Mohamad MS; Deris S; Zakaria Z. A review on the computational approaches for gene regulatory network construction. *Comput Biol Med.* **2014**, *48*, 55–65.
5. Park Y; Kellis M. Deep learning for regulatory genomics. *Nat Biotechnol.* **2015**, *33(8)*, 825–6.
6. Karr JR; Williams AH; Zucker JD; Raue A; Steiert B; Timmer J; Kreutz C; Wilkinson S; Allgood BA; Bot BM; et al. Summary of the DREAM8 Parameter Estimation Challenge: Toward Parameter Identification for Whole-Cell Models. *PLoS Comput Biol.* **2015**, *11(5)*, e1004096.
7. Yugi K; Kubota H; Toyoshima Y; Noguchi R; Kawata K; Komori Y; Uda S; Kunida K; Tomizawa Y; Funato Y; et al. Reconstruction of insulin signal flow from phosphoproteome and metabolome data. *Cell Rep.* **2014**, *8(4)*, 1171–83.
8. Karr JR; Sanghvi JC; Macklin DN; Gutschow MV; Jacobs JM; Bolival B Jr; Assad-Garcia N; Glass JI; Covert MW. A whole-cell computational model predicts phenotype from genotype. *Cell.* **2012**, *150(2)*, 389–401.
9. Milo R; Shen-Orr S; Itzkovitz S; Kashtan N; Chklovskii D; Alon U. Network motifs: simple building blocks of complex networks. *Science.* **2002**, *298(5594)*, 824–7.
10. Louvi A; Artavanis-Tsakonas S. Notch signalling in vertebrate neural development. *Nat Rev Neurosci.* **2006**, *7(2)*, 93–102.
11. Monk NA. Oscillatory expression of Hes1, p53, and NF-kappaB driven by transcriptional time delays. *Curr Biol.* **2003**, *13(16)*, 1409–13.
12. Zeiser S; Müller J; Liebscher V. Modeling the Hes1 oscillator. *J Comput Biol.* **2007**, *14(7)*, 984–1000.
13. Imayoshi I; Isomura A; Harima Y; Kawaguchi K; Kori H; Miyachi H; Fujiwara T; Ishidate F; Kageyama R. Oscillatory control of factors determining multipotency and fate in mouse neural progenitors. *Science.* **2013**, *342(6163)*, 1203–8.
14. Bai G; Sheng N; Xie Z; Bian W; Yokota Y; Benezra R; Kageyama R; Guillemot F; Jing N. Id sustains Hes1 expression to inhibit precocious neurogenesis by releasing negative autoregulation of Hes1. *Dev Cell.* **2007**, *13(2)*, 283–97.
15. Kageyama R; Ohtsuka T; Hatakeyama J; Ohsawa R. Roles of bHLH genes in neural stem cell differentiation. *Exp Cell Res.* **2005**, *306(2)*, 343–8.
16. Kageyama R; Ohtsuka T; Kobayashi T. Roles of Hes genes in neural development. *Dev Growth Differ.* **2008**, *50 Suppl 1*, S97–103.
17. Seki T., Sawamoto, K., Parent, J.M., Alvarez-Buylla, A, Eds. *Neurogenesis in the Adult Brain*, vol. 1. Tokyo: Springer; 2011.
18. Roybon L; Mastracci TL; Ribeiro D; Sussel L; Brundin P; Li JY. GABAergic differentiation induced by Mash1 is compromised by the bHLH proteins Neurogenin2, NeuroD1, and NeuroD2. *Cereb Cortex.* **2010**, *20(5)*, 1234–44.

19. Bhat KM; Maddodi N; Shashikant C; Setaluri V. Transcriptional regulation of human MAP2 gene in melanoma: role of neuronal bHLH factors and Notch1 signaling. *Nucleic Acids Res.* **2006**, *34(13)*, 3819–32.

20. Arimura N; Kaibuchi K. Neuronal polarity: from extracellular signals to intracellular mechanisms. *Nat Rev Neurosci.* **2007**, *8(3)*, 194–205.

21. Hand R; Bortone D; Mattar P; Nguyen L; Heng JI; Guerrier S; Boutt E; Peters E; Barnes AP; Parras C; et al. Phosphorylation of Neurogenin2 specifies the migration properties and the dendritic morphology of pyramidal neurons in the neocortex. *Neuron.* **2005**, *48(1)*, 45–62.

22. Shimizu T; Kagawa T; Inoue T; Nonaka A; Takada S; Aburatani H; Taga T. Stabilized beta-catenin functions through TCF/LEF proteins and the Notch/RBP-Jkappa complex to promote proliferation and suppress differentiation of neural precursor cells. *Mol Cell Biol.* **2008**, *28(24)*, 7427–41.

23. Schaefer CF; Anthony K; Krupa S; Buchoff J; Day M; Hannay T; Buetow KH. PID: the Pathway Interaction Database. *Nucleic Acids Res.* **2009**, *37*, D674–9.

24. Kelder T; van Iersel MP; Hanspers K; Kutmon M; Conklin BR; Evelo CT; Pico AR. WikiPathways: building research communities on biological pathways. *Nucleic Acids Res.* **2012**, *40*, D1301–7.

25. Funahashi A; Matsuoka Y; Jouraku A; Morohashi M; Kikuchi N; Kitano H. CellDesigner 3.5: A Versatile Modeling Tool for Biochemical Networks. *Proceedings of the IEEE.* **2008**, *96(8)*, 1254–1265

26. Kitano H; Funahashi A; Matsuoka Y; Oda K. Using process diagrams for the graphical representation of biological networks. *Nat Biotechnol.* **2005**, *23(8)*, 961-6.

27. Dräger A; Hassis N; Supper J; Schröder A; Zell A. SBMLsqueezer: a CellDesigner plug-in to generate kinetic rate equations for biochemical networks. *BMC Syst Biol.* **2008**, *2*, 39.

28. Milo R; Jorgensen P; Moran U; Weber G; Springer M. BioNumbers--the database of key numbers in molecular and cell biology. *Nucleic Acids Res.* **2010**, *38*, D750–3.

29. Bar-Even A; Noor E; Savir Y; Liebermeister W; Davidi D; Tawfik DS; Milo R. The moderately efficient enzyme: evolutionary and physicochemical trends shaping enzyme parameters. *Biochemistry.* **2011**, *50(21)*, 4402-10.

30. Legewie S; Herzel H; Westerhoff HV; Blüthgen N. Recurrent design patterns in the feedback regulation of the mammalian signalling network. *Mol Syst Biol.* **2008**, *4*, 190.

31. Hoops S; Sahle S; Gauges R; Lee C; Pahle J; Simus N; Singhal M; Xu L; Mendes P; Kummer U. COPASI--a COmplex PAthway SImulator. *Bioinformatics.* **2006**, *22(24)*, 3067–74.

32. Machné R; Finney A; Müller S; Lu J; Widder S; Flamm C. The SBML ODE Solver Library: a native API for symbolic and fast numerical analysis of reaction networks. *Bioinformatics.* **2006**, *22(11)*, 1406–7.

33. Petzold L. Automatic selection of methods for solving stiff and nonstiff systems of ordinary differential equations. *SIAM J Sci Stat Comput.* **1983**, *4*, 136–48.

34. Riccione KA; Smith RP; Lee AJ; You L. A synthetic biology approach to understanding cellular information processing. *ACS Synth Biol.* **2012**, *1(9)*, 389–402.

35. Eberhardt M; Lai X; Tomar N; Gupta S; Schmeck B; Steinkasserer A; Schuler G; Vera J. Third-kind encounters in biomedicine: immunology meets mathematics and informatics to become quantitative and predictive. *Methods Mol Biol.* **2016**, *1386*, 135-79.

36. Trinh HC; Le DH; Kwon YK. PANET: a GPU-based tool for fast parallel analysis of robustness dynamics and feed-forward/feedback loop structures in large-scale biological networks. *PLoS One.* **2014**, *9(7)*, e103010.

37. Patra S; Mohapatra A. Application of dynamic expansion tree for finding large network motifs in biological networks. *PeerJ.* **2019**, *7*, e6917.

38. Hirata H; Yoshiura S; Ohtsuka T; Bessho Y; Harada T; Yoshikawa K; Kageyama R. Oscillatory expression of the bHLH factor Hes1 regulated by a negative feedback loop. *Science.* **2002**, *298(5594)*, 840–3.

39. Kageyama R; Ohtsuka T; Kobayashi T. The Hes gene family: repressors and oscillators that orchestrate embryogenesis. *Development.* **2007**, *134(7)*, 1243–51.

40. Foltz DR; Santiago MC; Berechid BE; Nye JS. Glycogen synthase kinase-3beta modulates notch signaling and stability. *Curr Biol.* **2002**, *12(12)*, 1006-11.

41. Guha S; Cullen JP; Morrow D; Colombo A; Lally C; Walls D; Redmond EM; Cahill PA. Glycogen synthase kinase 3 beta positively regulates Notch signaling in vascular smooth muscle cells: role in cell proliferation and survival. *Basic Res Cardiol.* **2011**, *106(5)*, 773-85.

42. Jin YH; Kim H; Oh M; Ki H; Kim K. Regulation of Notch1/NICD and Hes1 expressions by GSK-3alpha/beta. *Mol Cells.* **2009**, *27(1)*, 15-9.

43. Kim WY; Wang X; Wu Y; Doble BW; Patel S; Woodgett JR; Snider WD. GSK-3 is a master regulator of neural progenitor homeostasis. *Nat Neurosci.* **2009**, *12(11)*, 1390-7.

44. Ye F; Chen Y; Hoang T; Montgomery RL; Zhao XH; Bu H; Hu T; Taketo MM; van Es JH; Clevers H; Hsieh J; Bassel-Duby R; Olson EN; Lu QR. HDAC1 and HDAC2 regulate oligodendrocyte differentiation by disrupting the beta-catenin-TCF interaction. *Nat Neurosci.* **2009**, *12(7)*, 829-38.

45. Zhang C; Zhang Z; Shu H; Liu S; Song Y; Qiu K; Yang H. The modulatory effects of bHLH transcription factors with the Wnt/beta-catenin pathway on differentiation of neural progenitor cells derived from neonatal mouse anterior subventricular zone. *Brain Res.* **2010**, *1315*, 1-10.

46. Peignon G; Durand A; Cacheux W; Ayrault O; Terris B; Laurent-Puig P; Shroyer NF; Van Seuningen I; Honjo T; Perret C; Romagnolo B. Complex interplay between b-catenin signalling and Notch effectors in intestinal tumorigenesis. *Gut.* **2011**, *60(2)*, 166-76.

47. Liu ZH; Dai XM; Du B. Hes1: a key role in stemness, metastasis and multidrug resistance. *Cancer Biol Ther.* **2015**, *16(3)*, 353-9.

48. Chasman D; Fotuhi Siahpirani A; Roy S. Network-based approaches for analysis of complex biological systems. *Curr Opin Biotechnol.* **2016**, *39*, 157-166.

49. McLeay RC; Bailey TL. Motif Enrichment Analysis: a unified framework and an evaluation on ChIP data. *BMC Bioinformatics.* **2010**, *11*, 165.

50. Morimoto M; Nishinakamura R; Saga Y; Kopan R. Different assemblies of Notch receptors coordinate the distribution of the major bronchial Clara, ciliated and neuroendocrine cells. *Development.* **2012**, *139(23)*, 4365–73.

51. Ramos C; Rocha S; Gaspar C; Henrique D. Two Notch ligands, Dll1 and Jag1, are differently restricted in their range of action to control neurogenesis in the mammalian spinal cord. *PLoS One.* **2010**, *5(11)*, e15515.

52. Cantone M; Küspert M; Reiprich S; Lai X; Eberhardt M; Göttle P; Beyer F; Azim K; Küry P; Wegner M; Vera J. A gene regulatory architecture that controls region-independent dynamics of oligodendrocyte differentiation. *Glia.* **2019**, *67(5)*, 825-843.

53. Hikichi T; Matoba R; Ikeda T; Watanabe A; Yamamoto T; Yoshitake S; Tamura-Nakano M; Kimura T; Kamon M; Shimura M; et al. Transcription factors interfering with dedifferentiation induce cell type-specific transcriptional profiles. *Proc Natl Acad Sci U S A.* **2013**, *110(16)*, 6412–7.

54. Real C; Glavieux-Pardanaud C; Le Douarin NM; Dupin E. Clonally cultured differentiated pigment cells can dedifferentiate and generate multipotent progenitors with self-renewing potential. *Dev Biol.* **2006**, *300(2)*, 656–69.

55. van Groningen T; Akogul N; Westerhout EM; Chan A; Hasselt NE; Zwijnenburg DA; Broekmans M; Stroeken P; Haneveld F; Hooijer GKJ; et al. A NOTCH feed-forward loop drives reprogramming from adrenergic to mesenchymal state in neuroblastoma. *Nat Commun.* **2019**, *10(1)*, 1530.